

---

# VARIATIONAL APPROACH FOR JOB SHOP SCHEDULING\*

---

**Seung Heon Oh**  
 Republic of Korea Navy  
 Gyeryong  
 suenghuny@snu.ac.kr

**Jiwon Baek, Ki Young Cho, Hee Chang Yoon**  
 Department of Naval Architecture and Ocean Engineering  
 Seoul National University  
 Seoul

**Jong Hun Woo**  
 Department of Naval Architecture and Ocean Engineering  
 Seoul National University  
 Seoul  
 Research Institute of Marine Systems Engineering  
 Seoul National University  
 Seoul  
 j.woo@snu.ac.kr

## ABSTRACT

This paper proposes a novel Variational Graph-to-Scheduler (VG2S) framework for solving the Job Shop Scheduling Problem (JSSP), a critical task in manufacturing that directly impacts operational efficiency and resource utilization. Conventional Deep Reinforcement Learning (DRL) approaches often face challenges such as non-stationarity during training and limited generalization to unseen problem instances because they optimize representation learning and policy execution simultaneously. To address these issues, we introduce variational inference to the JSSP domain for the first time and derive a probabilistic objective based on the Evidence of Lower Bound (ELBO) with maximum entropy reinforcement learning. By mathematically decoupling representation learning from policy optimization, the VG2S framework enables the agent to learn robust structural representations of scheduling instances through a variational graph encoder. This approach significantly enhances training stability and robustness against hyperparameter variations. Extensive experiments demonstrate that the proposed method exhibits superior zero-shot generalization compared with state-of-the-art DRL baselines and traditional dispatching rules, particularly on large-scale and challenging benchmark instances such as DMU and SWV.

## 1 Introduction

Job shop scheduling problem (JSSP) is a fundamental challenge in manufacturing, directly impacting the operational efficiency and resource utilization of various manufacturing systems. While traditional methods—such as heuristics, meta-heuristics, and mathematical programming—have been widely used, their need for instance-specific optimization often limits their flexibility in dynamic shop-floor environments. Recently, Deep Reinforcement Learning (DRL) has emerged as a powerful alternative in various scheduling domains, including manufacturing [1, 2, 3], logistics [4, 5], traffic control [6, 7], and defense [8, 9]. By leveraging learned policies, it achieves both superior performance and strong generalization across different scenarios. Unlike conventional approaches that require time-consuming re-optimization for every new task, a trained DRL model can be immediately deployed to diverse problem instances, providing the operational robustness necessary for real-time manufacturing decision-making.

The core of this capability lies in how the model perceives and represents the complex, interconnected state of the production environment. Therefore, a significant portion of recent research has focused on designing effective neural network (NN) architectures that can transform raw job-shop data into meaningful features for decision-making. From an architectural perspective, early studies applying DRL to JSSP utilized Multi-Layered Perceptron (MLP) [10, 11, 12, 2]

---

\*This paper includes supplementary material.

or Convolutional Neural Network (CNN) [13, 14, 15]. These NNs learn representations of JSSP instances and states in vector or matrix forms to extract useful hidden information for problem solving. However, representing the constraint relationships inherent in JSSP using vectors and matrices posed difficulties, and these approaches had limitations in not being agnostic to varying problem sizes [16].

These limitations arise from the inherent nature of constraint relationships in JSSP. JSSP constraints are represented as a disjunctive graph, embodying unique topological relationships that cannot be readily captured in Euclidean space [17]. This characteristic distinguishes JSSP from other combinatorial optimization problems such as the traveling salesman problem and vehicle routing problem. Indeed, numerous algorithms—including the fast branch and bound algorithm [18] and the shifting bottleneck procedure [19]—have been developed specifically to exploit this disjunctive graph structure. Consequently, DRL methods also require the capability to effectively handle such graph structures.

The key to leveraging this topological structure in the context of DRL lies in effective representation learning. Graph Neural Networks (GNNs) are specifically designed to process graph-structured data, making them particularly well-suited for capturing complex relational patterns and dependencies inherent in graph topologies. This capability has made GNN a natural framework for learning representations of topologies in JSSP, where operations and machines form intricate networks of precedence and resource constraints. GNN-based studies in JSSP can be categorized along two key aspects related to representation learning: (1) graph representation and (2) architecture design. *Graph representation* defines **what** information is encoded: how JSSP entities (operations, machines) and relationships (precedence, disjunctive constraints) are structured as graph topology and node/edge features. *Architecture design* defines **how** this information is processed: which GNN architectures and training methodologies extract representations and learn policies.

In terms of *graph representation*, the field has shown systematic evolution through problem-driven designs. [16] and [20] propose a foundational framework representing operations as featured nodes, which has been widely adopted in subsequent works [21, 22, 23, 24, 25, 26]. Building on this foundation, researchers have developed specialized representations for diverse JSSP variants: masking mechanisms for invalid operations [26], heterogeneous graphs for dynamic environments [24, 23, 25], stitched disjunctive graphs for distributed multi-factory settings [22, 21, 27], and heterogeneous representations for flexible job shop problems [28, 29, 30]. These studies have effectively expanded the scope of JSSP modeling by developing versatile graph structures that can encode the unique constraints of each problem variant.

In terms of *architecture design*, existing works have primarily focused on adopting existing GNN architectures. Various GNN architectures have been applied—including Graph Isomorphism Network (GIN) [20, 21, 22, 23, 26, 27], standard GNN layers [16], random walk embeddings [31], and Graph Attention Network (GAT) [24, 25, 32]. Some recent works [31, 32] have explored graph-to-sequence architectures that structurally decouple the processing of static graph features and dynamic scheduling decisions. Regardless of these architectural variations, all these methods are trained in an end-to-end manner. This paradigm enables the joint optimization of representation-level feature extraction and policy-level task execution, ensuring that the learned embeddings are inherently aligned with the scheduling objectives.

While recent DRL approaches show promise in the JSSP domain, they rely on the optimistic expectation that NNs have the representational capability to effectively generalize across diverse JSSP instances. In practice, however, the effectiveness of this approach remains limited. While these models show potential in classical JSSP settings, even state-of-the-art approaches [33, 32, 26] experience significant performance degradation under minor deviations from those conditions. This is evidenced by their reduced performance on the Demirkol et al. (DMU) and Storer et al. (SWV) benchmark datasets, which are widely recognized for their inherent difficulty [34]. This limited generalization is problematic for real-world manufacturing systems, which inherently involve high variability and complexity.

This shortcoming stems from the limitation of the standard end-to-end learning paradigm. Specifically, when coupled with GNNs, well-known for their graph representation capabilities, the architecture is expected to automatically extract problem representations and optimize scheduling policies simultaneously. However, optimizing for policy performance does not necessarily yield a robust structural representation. The concurrent evolution of representation and policy introduces reciprocal non-stationarity, where any update in one component shifts the optimization landscape for the other. This phenomenon leads to unstable training, extreme sensitivity to hyperparameters, and degradation of performance [35]. To bridge this gap, we propose a variational approach that explicitly decouples representation learning from policy optimization, with the following contributions:

- We derive a rigorous probabilistic objective based on the Evidence of Lower Bound (ELBO) with maximum entropy reinforcement learning (RL) for JSSP. This provides a framework to handle the latent stochasticity inherent in scheduling, facilitating robust representation and generalization across unseen production scenarios.
- We introduce VG2S, a novel Variational Graph-to-Scheduler framework that integrates a variational graph encoder with a sequence-based policy decoder. Our approach mitigates the non-stationarity common in standard end-to-end models, thereby enhancing training stability and robustness to hyperparameters.

- We demonstrate structural awareness and superior zero-shot generalization through extensive experiments. UMAP analysis confirms that the latent space clusters instances by topological similarity even before policy training. Consequently, our approach significantly outperforms state-of-the-art DRL baselines and traditional dispatching rules on large-scale benchmarks, including DMU and SWV.
- To the best of our knowledge, this is the first study to demonstrate that variational inference facilitates robust representation learning in JSSP. Our experiments confirm that through variational representation learning, our framework effectively compresses essential characteristics into a structured latent space, facilitating enhanced training stability and robust zero-shot generalization.

## 2 Problem definition

A JSSP is characterized by the triple  $\langle \mathcal{J}, \mathcal{O}, \mathcal{M} \rangle$ , which comprises a set of  $n$  jobs  $\mathcal{J} = \{J_1, \dots, J_n\}$ , a set of  $m$  machines  $\mathcal{M} = \{M_1, \dots, M_m\}$ , and a set of operations  $\mathcal{O}$ . Each job  $J_j \in \mathcal{J}$  is subject to precedence constraints, requiring its constituent operations to be processed in a fixed, predetermined sequence. Furthermore, every operation  $O_{ij}$  is pre-assigned to a specific machine  $M_i \in \mathcal{M}$  and is associated with a processing duration  $p_{ij}$ , where the index  $j$  identifies its parent job.

The objective is to minimize the makespan  $C_{\max}$ , defined as the total duration required to complete all jobs. This optimization is conducted under several standard assumptions: operations are non-preemptive, each machine can process only one operation at a time, and all jobs are available simultaneously at the start of the schedule. Furthermore, any time associated with machine setup or job transportation is considered negligible.

A JSSP instance is formally represented as a disjunctive graph  $G = (V, C \cup D)$ , where  $V$  denotes the set of all operations. The set of conjunctive edges  $C$  encodes precedence constraints; specifically, a directed edge  $(u, v) \in C$  indicates that operation  $u$  must be completed before operation  $v$  can begin within the same job. The set of disjunctive edges  $D$  represents machine-sharing relations, where an undirected edge connects any two operations required to be processed on the same machine, signifying that their execution order must be determined to avoid resource conflicts.

$$\begin{aligned} & \text{minimize} && C_{\max} \\ & \text{subject to} && y_{ij} - y_{kj} \geq p_{kj} \quad \forall (k, j) \rightarrow (i, j) \in C \\ & && y_{ij} - y_{il} \geq p_{il} \quad \text{or} \quad y_{il} - y_{ij} \geq p_{ij} \\ & && \forall (i, j) \text{ and } (i, l), \quad i = 1, \dots, m \\ & && C_{\max} - y_{ij} \geq p_{ij} \quad \forall (i, j) \in V \\ & && y_{ij} \geq 0 \quad \forall (i, j) \in V \end{aligned}$$

where the decision variable  $y_{ij}$  denotes the starting time of operation  $O_{ij}$ , and  $p_{ij}$  is its processing time.

## 3 Representing JSSP instance

To effectively model a JSSP instance, we distinguish between its static attributes and dynamic characteristics. Static information, representing the invariant topology of the problem, is modeled as a heterogeneous graph in Section 3.1. Dynamic information, elaborated in Section 3.2, captures the state transitions of the evolving partial schedule.

### 3.1 Static information: instance-specific features

We represent each JSSP instance as a heterogeneous graph  $G = (\mathcal{V}, (\mathcal{E}_1, \mathcal{E}_2, \mathcal{E}_3))$ , where nodes  $v \in \mathcal{V}$  denote operations. In this graph, each node  $v \in \mathcal{V}$  represents an operation and is associated with six distinct features of [32]. The edges  $\mathcal{E}_1, \mathcal{E}_2$ , and  $\mathcal{E}_3$  represent precedence, successor, and machine-sharing dependencies. To ensure generalization across diverse JSSP instances, operation features are normalized to reflect relative values within each instance. These features  $(\mathbf{x}_{ij}^1, \dots, \mathbf{x}_{ij}^6)$  capture instance-specific semantics as follows:

$$\begin{aligned} \mathbf{x}_{ij}^1 &= \frac{p_{ij}}{\sum_{M_{i'} \in \mathcal{M}} p_{i'j}}, & \mathbf{x}_{ij}^2 &= \frac{p_{ij}}{\max_{M_{i'} \in \mathcal{M}} p_{i'j}}, & \mathbf{x}_{ij}^3 &= \frac{p_{ij}}{\sum_{J_{j'} \in \mathcal{J}} p_{ij'}} \\ \mathbf{x}_{ij}^4 &= \frac{\sum_{M_{i'} \in \mathcal{A}_{ij}} p_{i'j}}{\sum_{M_{i'} \in \mathcal{M}} p_{i'j}}, & \mathbf{x}_{ij}^5 &= \frac{|\mathcal{A}_{ij}|}{|\mathcal{M}|}, & \mathbf{x}_{ij}^6 &= \frac{\sum_{M_{i'} \in \mathcal{M}} p_{i'j}}{\max_{j'} \sum_{M_{i'} \in \mathcal{M}} p_{i'j'}} \end{aligned}$$

$\mathcal{A}_{ij}$  denotes the set of machines comprising the current machine for  $O_{ij}$  and all machines previously visited by job  $J_j$ . The node set  $\mathcal{V}$  is represented as a feature matrix  $\mathbf{X} \in \mathbb{R}^{N_O \times 6}$ , where each row  $\mathbf{x}_u = (\mathbf{x}_u^1, \dots, \mathbf{x}_u^6)$  is the feature vector

of operation  $O_u$ . The total number of nodes is defined as  $N_O = nm + 2$  to account for two additional dummy nodes: a source node  $(0, 0, 0, 0, 0, 0)$  representing the start of the schedule, and a sink node  $(0, 0, 1, 1, 1, 0)$  representing its completion.  $\mathcal{N}_{\mathcal{E}_\cdot}(u)$  defines the set of neighboring operations of  $O_u$  connected via edges in  $\mathcal{E}_\cdot$ . Specifically:

- $\mathcal{N}_{\mathcal{E}_1}(u)$ : the precedent operation index of  $O_u$
- $\mathcal{N}_{\mathcal{E}_2}(u)$ : the successor operation index of  $O_u$
- $\mathcal{N}_{\mathcal{E}_3}(u)$ : machine-sharing operation indices of  $O_u$

**Remarks:** We adopt two notations for operations:  $O_{ij}$  represents job  $j$  on machine  $i$  to highlight specific job-machine associations, while  $O_u$  serves as a simplified single-index notation within the context of the NN architecture.

### 3.2 Dynamic information: state features

The JSSP instance  $G$  is processed by the initial state function  $g_0$  to produce the initial state  $s_1 = g_0(G)$ . The environment then follows the transition dynamics  $s_{t+1} = g(s_t, a_t, G)$ , where  $s_t$  denotes the state at each decoding timestep  $t$  and  $a_t$  represents the action indicating the selected operation at timestep  $t$ . Upon the state transition, the selected action is assigned to the designated machine and executed immediately as the machine becomes available, ensuring zero unnecessary idle time (i.e., semi-active scheduling; Details are provided in the Supplementary Material A).

We define  $\mathcal{A}(s_t)$  as the set of available operations at state  $s_t$ . The state features  $s_{1,t}^{ij}$  and  $s_{2,t}^{ij}$  denote the earliest start and finish times for each action  $a_t = O_{ij} \in \mathcal{A}(s_t)$  and are defined as follows:

$$\begin{aligned} s_{1,t}^{ij} &= \max\{\mathbf{m}_t^i, \mathbf{j}_t^j\} \\ s_{2,t}^{ij} &= \max\{\mathbf{m}_t^i, \mathbf{j}_t^j\} + p_{ij} \end{aligned}$$

The dynamic variables  $\mathbf{m}_t^i$  and  $\mathbf{j}_t^j$  represent the ready times for machine  $i$  and job  $j$  at time  $t$ , respectively (Details of  $\mathbf{m}_t^i$  and  $\mathbf{j}_t^j$  are provided in the Supplementary Material A). Here,  $s_{1,t}^{ij}$  and  $s_{2,t}^{ij}$  are set to zero whenever an operation  $O_{ij}$  is outside the set  $\mathcal{A}(s_t)$ . To ensure consistent input scales for the model, we normalize these values into the range between 0 and 1, using  $\max_{ij} s_{1,t}^{ij}$  and  $\max_{ij} s_{2,t}^{ij}$  as the scaling factors for each feature. We employ the *efficient lower bound* from [32] by utilizing state features  $s_{3,t}^{ij}$  and  $s_{4,t}^{ij}$  as follows:

$$\begin{aligned} s_{3,t}^{ij} &= \max\{\mathbf{m}_i(\tilde{s}^{ij}(s_t)) + \mathbf{r}_i(\tilde{s}^{ij}(s_t)), \mathbf{j}_j(\tilde{s}^{ij}(s_t)) + \mathbf{r}_j(\tilde{s}^{ij}(s_t))\} \\ s_{4,t}^{ij} &= \max_{\substack{J_j \in \mathcal{J} \\ O_{\hat{j}} \in \mathcal{A}(\tilde{s}^{ij}(s_t))}} \max\{\mathbf{m}_i(\tilde{s}^{ij}(s_t)) + \mathbf{r}_i(\tilde{s}^{ij}), \mathbf{j}_{\hat{j}}(\tilde{s}^{ij}(s_t)) + \mathbf{r}_{\hat{j}}(\tilde{s}^{ij}(s_t))\} \end{aligned}$$

Here, the variables  $\mathbf{m}_i(s)$  and  $\mathbf{j}_j(s)$  correspond to the machine  $i$  and job  $j$  ready times in state  $s$ , while  $\mathbf{r}_i(s)$  and  $\mathbf{r}_j(s)$  signify their respective remaining processing times in state  $s$ . Despite being less restrictive than standard bounds, this formulation is selected for its straightforward implementation and minimal computational requirements during execution. The successor state resulting from the selection of operation  $O_{ij}$  at  $s_t$  is denoted by  $\tilde{s}^{ij}(s_t)$ . In cases where  $O_{ij}$  is the terminal operation of job  $J_j$ , the state feature  $s_{3,t}^{ij}$  along with the terms  $\mathbf{m}_i(\tilde{s}^{ij}(s_t)) + \mathbf{r}_i(\tilde{s}^{ij}(s_t))$  and  $\mathbf{r}_{\hat{j}}(\tilde{s}^{ij}(s_t)) + \mathbf{r}_{\hat{j}}(\tilde{s}^{ij}(s_t))$  are defined to be zero. Additionally, state features  $s_{5,t}^{ij}$  and  $s_{6,t}^{ij}$  are introduced to capture the global progress of the scheduling process as follows:

$$\begin{aligned} s_{5,t}^{ij} &= \max_{J_{\hat{j}} \in \mathcal{J}} \mathbf{C}_{\hat{j}}(\tilde{s}^{ij}(s_t)) \\ s_{6,t}^{ij} &= \text{mean}_{J_{\hat{j}} \in \mathcal{J}} \mathbf{C}_{\hat{j}}(\tilde{s}^{ij}(s_t)) \end{aligned}$$

Here,  $\mathbf{C}_{\hat{j}}(\tilde{s}^{ij})$  denotes the number of completed operations for job  $J_{\hat{j}}$  in the state  $\tilde{s}^{ij}(s_t)$  transitioned by selecting operation  $O_{ij}$ . Specifically,  $s_{5,t}^{ij}$  represents the maximum number of completed operations among all jobs, indicating the progress of the most advanced job. Meanwhile,  $s_{6,t}^{ij}$  represents the average number of completed operations across all jobs, providing a global measure of the overall completion status of the entire instance. The state features  $s_{5,t}^{ij}$  and  $s_{6,t}^{ij}$  are normalized by the total number of machines  $m$ . Consequently, the state feature vector  $s_t^u \in \mathbb{R}^6$  of  $O_u$  indicates  $(s_{1,t}^u, s_{2,t}^u, s_{3,t}^u, s_{4,t}^u, s_{5,t}^u, s_{6,t}^u)$ .

## 4 Evidence of lower bound with maximum entropy RL for JSSP

While state transitions within a single JSSP instance are deterministic, achieving robust generalization over diverse scheduling instances requires addressing the uncertainty inherent across the problem space. To model this uncertainty, we introduce the distribution of instances  $p(G)$ , representing the likelihood of encountering a specific problem instance  $G$ , and the conditional probability of achieving optimality  $p(O = 1|G)$ . Here,  $O$  denotes a binary random variable indicating whether optimality is achieved. Consequently, the objective function is formulated as maximizing the joint probability  $p(G, O = 1)$  as follows:

$$p(G, O = 1) = p(G) \cdot p(O = 1|G) \quad (1)$$

This objective function mathematically formalizes the goal of robust generalization by integrating the instance distribution  $p(G)$ , thereby preventing overfitting to specific instances and promoting consistent performance across a wide range of problems. By marginalizing  $p(G, O = 1)$  over the latent variable  $z$  and the action sequence  $a$ , we can express the lower bound on the log-likelihood of the objective function as (2) – (3) (Derivations are provided in the Supplementary Material B).

$$\log p(G, O) = \log \sum_{z, a} [p(G, O, z, a) \cdot \frac{q(z, a|G)}{q(z, a|G)}] \quad (2)$$

$$\geq \underbrace{\mathbb{E}_{z, a \sim q} [\log p(G|z)] - D_{\text{KL}}[q(z|G) || p(z)]}_{\text{Reconstruction loss term}} + \underbrace{\mathbb{E}_{z, a \sim q} [Q(z, a) - \log \pi(a|z, G) + \log p(a|G, z)]}_{\text{Policy loss term}} \quad (3)$$

Here, the posterior  $q(z, a|G)$  factorizes into the posterior  $q(z|G)$  and the policy  $\pi(a|z, G)$ :  $q(z, a|G) = q(z|G) \cdot \pi(a|z, G)$ . The derivation in (2) – (3) assumes that  $p(O = 1|G, z, a)$  is proportional to the exponential of  $Q(z, a)$ :  $p(O = 1|G, z, a) \propto \exp Q(z, a)$ . Here,  $Q(z, a)$  represents the scheduling objective score (e.g., negative makespan) for a given latent variable  $z$  and action sequence  $a$ . (3) can be decomposed into ELBO consisting of two terms: reconstruction loss and policy loss term. This is a special case of variational inference with maximum entropy RL [35]. By maximizing this ELBO, we can effectively optimize the original objective function of (1). In particular, under the uniform prior assumption for  $\log p(a|G, z)$ , the policy loss term reduces to a maximum entropy RL formulation with baseline, corresponding to the policy gradient with maximum entropy in (4).

$$J(\pi) = \mathbb{E}_{z \sim q} \mathbb{E}_{a \sim \pi} [Q(z, a) - V(z) - \log \pi(a|z, G)] \quad (4)$$

where  $J(\pi)$  is the maximum entropy RL objective. This analysis provides theoretical justification for integrating variational representation learning with maximum entropy RL-based policy optimization (Derivations are provided in the Supplementary Material B).

## 5 Variational graph-to-scheduler framework for JSSP

We propose a Variational Graph-to-Scheduler (VG2S) framework for the JSSP, which integrates the aforementioned theoretical insights with a Variational Autoencoder (VAE) approach [36] and a graph-to-sequence architecture [31, 12]. The proposed framework consists of variational graph encoder (Section 5.1) and policy decoder (Section 5.2), as illustrated in Fig. 1. The training process is divided into two stages: variational representation learning and policy learning. During the variational representation learning stage, by optimizing the ELBO—specifically the reconstruction loss—the model is compelled to distill the complex structural dependencies and constraints of the JSSP into a highly informative and compact latent space. This process yields a more robust and expressive representation of the problem instances, which ultimately enhances the decision-making performance of the policy decoder. In the policy learning stage, the maximum entropy policy loss is optimized using trajectories generated during schedule construction.

### 5.1 Variational graph encoder

The variational graph encoder is composed of a representation network (Section 5.1.1) for inferring latent representations, a latent space model (Section 5.1.2) for capturing the distributional properties of the learned representations, and a generative network (Section 5.1.3) for graph reconstruction. It is crucial to emphasize that while the framework incorporates a generative architecture, its primary objective is not the direct utilization of reconstructed graph instances. Instead, we capitalize on the representation learning capacity inherent in the generative training process. The overall network architecture is illustrated in Fig. 2.

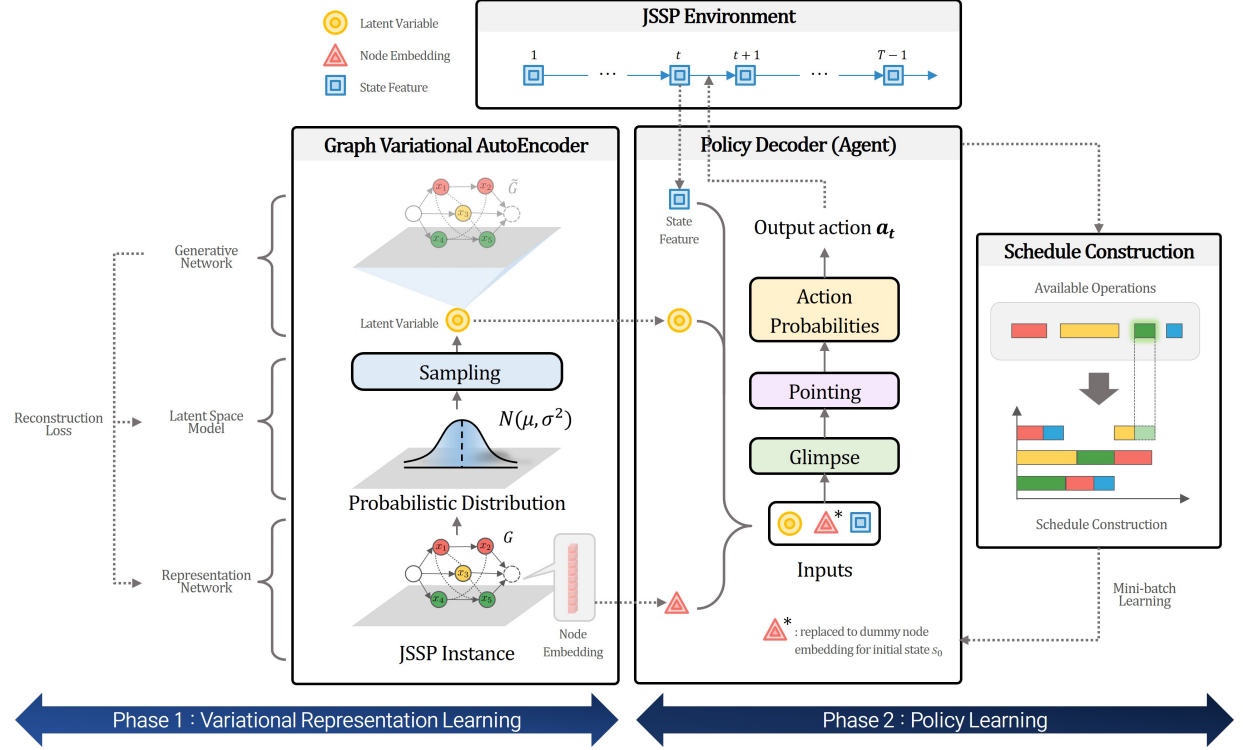


Figure 1: Overview of the proposed VG2S framework

### 5.1.1 Representation network

In our architecture, A JSSP instance  $G$  is fed into the representation network  $f_{\phi_1}$  parametrized by  $\phi_1$ , which outputs node embeddings  $h$  as follows:

$$h = f_{\phi_1}(G)$$

The representation network consists of two main components: a feature embedding layer and GNN layers. The feature embedding layer applies MLP to map input node features  $\mathbf{X} \in \mathbb{R}^{N_O \times 6}$  from dimension 6 to  $d_{\text{graph}}$ :

$$H_{\text{embed}} = \text{MLP}_{\text{embed}}(\mathbf{X})$$

where  $H_{\text{embed}} \in \mathbb{R}^{N_O \times d_{\text{graph}}}$  is the embedded feature matrix whose  $u$ -th row represents the node embedding of  $O_u$ . GNN layers employ multi-head GAT [37], which processes heterogeneous graphs with multiple edge types through multi-head attention mechanisms. For each edge type  $e \in \{1, 2, 3\}$  and attention head  $m \in \{1, 2, \dots, M_{\text{head}}\}$ , the layer computes:

$$H_{\text{linear}}^{(e,m)} = H_{\text{embed}} W_s^{(e,m)}$$

$W_s^{(e,m)} \in \mathbb{R}^{d_{\text{graph}} \times d_{\text{graph}}}$  is the learnable weight matrix for edge type  $e$  and head  $m$ . The attention mechanism computes edge-specific attention coefficients:

$$a_{uv}^{(e,m)} = \text{LeakyReLU}(a_1^{(e,m)\top} H_{\text{linear},u}^{(e,m)} + a_2^{(e,m)\top} H_{\text{linear},v}^{(e,m)}), \quad \alpha_{uv}^{(e,m)} = \frac{\exp(a_{uv}^{(e,m)})}{\sum_{v' \in \mathcal{N}_{\mathcal{E}_e}(u)} \exp(a_{uv'}^{(e,m)})}$$

where  $H_{\text{linear},u}^{(e,m)}$  is the element corresponding to node  $u$  in  $H_{\text{linear}}^{(e,m)}$  and  $a_1^{(e,m)}, a_2^{(e,m)} \in \mathbb{R}^{d_{\text{graph}}}$  are learnable attention parameters. The output of node  $u$  for edge type  $e$  and head  $m$ , denoted as  $H_{\text{edge},u}^{(e,m)} \in \mathbb{R}^{d_{\text{latent}}}$ , is computed as follows:

$$H_{\text{edge},u}^{(e,m)} = \text{ELU} \left( \sum_{v' \in \mathcal{N}_{\mathcal{E}_e}(u)} \alpha_{uv'}^{(e,m)} H_{\text{linear},v'}^{(e,m)} \right)$$

and then concatenated to form  $H_{\text{edge},u}^{(e)} \in \mathbb{R}^{Md_{\text{latent}}}$  as:

$$H_{\text{edge},u}^{(e)} = \text{Concat}(H_{\text{edge},u}^{(e,1)}, \dots, H_{\text{edge},u}^{(e,M)})$$

The embeddings  $H_{\text{edge},u}^{(e)}$  computed for each edge type are concatenated into  $H_{\text{combined},u} \in \mathbb{R}^{3Md_{\text{latent}}}$  as follows:

$$H_{\text{combined},u} = \text{Concat}(H_{\text{edge},u}^{(1)}, H_{\text{edge},u}^{(2)}, H_{\text{edge},u}^{(3)})$$

Note that  $H_{\text{edge}}^{(e)}$  in Fig. 2 denotes the collection of  $H_{\text{edge},u}^{(e)}$  for all  $u$ . We then employ a linear transformation to project the concatenated features back to the latent dimension  $d_{\text{latent}}$ :

$$H_{\text{proj},u} = \text{Linear}(H_{\text{combined},u})$$

where  $H_{\text{proj},u} \in \mathbb{R}^{d_{\text{latent}}}$ . The aggregation function, denoted as  $\text{Aggr}(\cdot)$  computes the node embedding  $h_u$  by combining Approximate Personalized Propagation of Neural Predictions (APPNP), residual connections, and batch normalization. The specific combination is treated as a hyperparameter.

$$h_u = \text{Aggr}(H_{\text{proj},u})$$

The node embeddings  $h \in \mathbb{R}^{NO \times d_{\text{latent}}}$  are the collection of  $h_u \in \mathbb{R}^{d_{\text{latent}}}$  for all  $u$ .

### 5.1.2 Latent space model

The latent space model implements a variational framework with a Gaussian prior distribution having mean 0 and standard deviation  $\sigma_p$ :

$$p(z) = N(0, \sigma_p^2 I)$$

where  $\sigma_p$  is 1 and  $I$  is identity matrix. The latent space model implements a variational framework where the posterior distribution  $q_{\phi}(z|G)$  is modeled as a diagonal Gaussian with instance-dependent mean and variance. Our architecture employs a specialized network to jointly learn both parameters:

$$q_{\phi}(z|G) = \mathcal{N}(\mu_z, \text{diag}(\sigma_z^2))$$

To capture the complex dependencies between the graph structure and latent variables, the aggregated node embeddings  $h$  are first processed by a shared feature extractor, followed by two separate heads. Specifically, a shared MLP first maps the input to an intermediate latent representation, which is then split into two distinct feature vectors,  $h_{\mu}$  and  $h_{\sigma}$ :

$$[h_{\mu}, h_{\sigma}] = \text{MLP}_{\text{shared}}(h)$$

where  $[\cdot, \cdot]$  denotes the splitting operation along the feature dimension. Subsequently, these features are passed through specific MLP heads to predict the mean and standard deviation:

$$\begin{aligned} \mu_z &= \text{MLP}_{\mu}(h_{\mu}) \\ \sigma_z &= \text{Softplus}(\text{MLP}_{\sigma}(h_{\sigma})) + \epsilon_{\text{min}} \end{aligned}$$

where  $\text{Softplus}(x) = \log(1 + e^x)$  ensures positive standard deviation, and  $\epsilon_{\text{min}}$  (set to  $1e^{-5}$ ) is a small constant for numerical stability. Finally, the latent variable  $z$  is sampled using the reparameterization trick:

$$z = \mu_z + \epsilon \odot \sigma_z, \quad \epsilon \sim \mathcal{N}(0, I)$$

This hierarchical architecture allows the model to extract shared structural features before refining them into the specific statistics required for the variational distribution.

### 5.1.3 Generative network

Generative component  $p_{\psi}(G|z)$ , parametrized with  $\psi$  serves as a generative model for graph reconstruction. In practice, this is implemented via a deterministic function  $g_{\psi}(z)$  that outputs node probabilities  $\mathbf{P}_{\text{node}}$  (representing node features) and edge connection probabilities  $\mathbf{P}_{\text{edge}}$ , where  $\mathbf{P}_{\text{node}} \in [0, 1]^{nm \times 6}$  and  $\mathbf{P}_{\text{edge}} \in [0, 1]^{nm \times nm}$ :

$$G \sim p_{\psi}(G|z) \text{ via } \mathbf{P}_{\text{node}}, \mathbf{P}_{\text{edge}} = g_{\psi}(z)$$

The generative network employs 1D transposed convolutions to generate graph structures from latent representations. The architecture consists of:

$$\mathbf{z}^{(p)} = \begin{cases} \text{Linear}(z) & \text{if } p = 0 \\ \text{ConvTranspose}_{d_{p-1} \rightarrow d_p}(\mathbf{z}^{(p-1)}) & \text{otherwise} \end{cases}$$

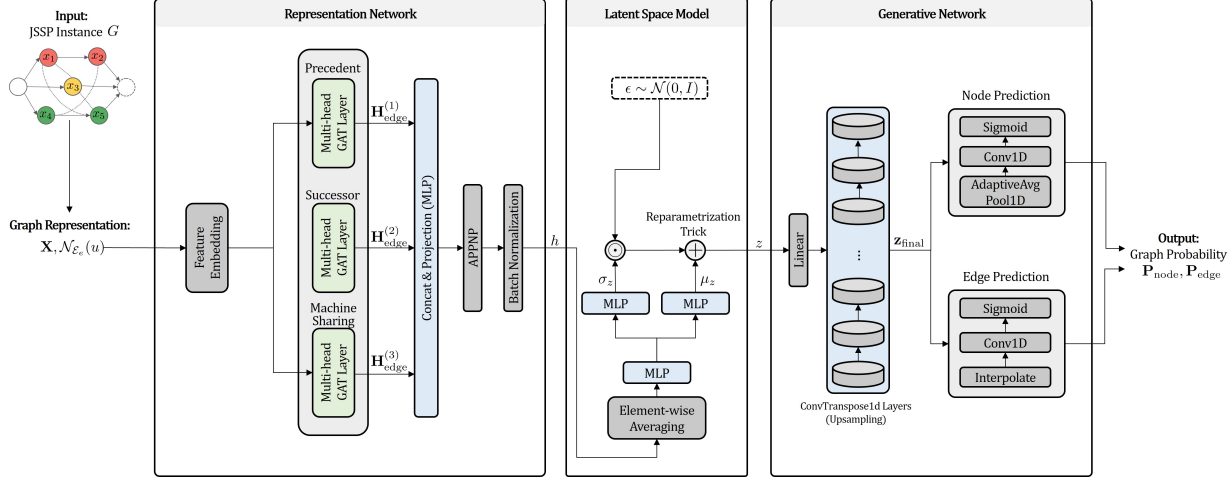


Figure 2: Architecture of variational graph encoder

For  $p = 0$ , the linear transformation maps  $z$  to an initial feature representation of dimension  $d_0$  and reshapes it to  $\mathbf{z}^{(0)} \in \mathbb{R}^{d_0 \times 1}$  with sequence length 1. Subsequently, the  $p$ -th transposed convolution operation  $\text{ConvTranspose}_{d_{p-1} \rightarrow d_p}$  (with kernel size 4, stride 2, and padding 1) progressively reduces the channel dimension from  $d_{p-1}$  to  $d_p$  while doubling the sequence length at each layer. After  $P$  transposed convolution layers, the sequence length exponentially grows to  $2^P$ . This hierarchical upsampling process generates increasingly detailed structural representations from the compressed latent space. The final output  $\mathbf{z}_{\text{final}} \in \mathbb{R}^{d_P \times N_*}$  has channel dimension  $d_P$  and sequence length  $N_* = n^*m^*$ , where  $n^*$  and  $m^*$  represent the maximum number of jobs and machines that can be encountered across problem instances. For node prediction, adaptive average pooling resizes  $\mathbf{z}_{\text{final}}$  to match the desired node count before convolution:

$$\mathbf{P}_{\text{node}} = \sigma(\text{Conv1D}(\text{AdaptiveAvgPool1D}(\mathbf{z}_{\text{final}}, N_*)))$$

where  $\sigma$  is the sigmoid activation function and  $\mathbf{P}_{\text{node}} \in [0, 1]^{N \times 6}$  represents the prediction of node features, with 6 indicating the number of columns of  $\mathbf{X}$ . For edge prediction, the sequence is interpolated to match the size  $N_*^2$ :

$$\mathbf{P}_{\text{edge}} = \sigma(\text{Conv1D}(\text{Interpolate}(\mathbf{z}_{\text{final}}, \text{size} = N_*^2)))$$

where  $\mathbf{P}_{\text{edge}} \in [0, 1]^{N \times N \times 3}$  represents edge probabilities reshaped from the  $N_*^2$ -length sequence,  $d_h$  is the hidden dimension, and 3 denotes the number of edge types.

## 5.2 Policy decoder

The policy decoder generates the schedule constructively using  $z$  and  $h$  while interacting with the JSSP environment. The action is selected from a policy function  $\pi$ , which is defined as follows:

$$\pi_{\theta}(a|z, G) = \prod_{t=1}^{nm} p_{\theta}(a_t|z, s_t, a_{t-1})$$

where action sequence  $a = (a_1, a_2, \dots, a_{nm})$  consists of actions  $a_t$  at each timestep  $t$ . The policy decoder representing the policy interacts with the JSSP environment iteratively by observing the state and selecting actions. The policy decoder inputs for selecting action  $a_t$  at time step  $t$  consist of the context embedding ( $\mathbf{c}_t$ ) and node-specific state embeddings ( $\mathbf{k}_t^u$ ) as follows:

$$\mathbf{c}_t = \text{Concat}(z, h_{a_{t-1}}), \quad \mathbf{k}_t^u = \text{Concat}(h_u, \text{MLP}(s_t^u))$$

where  $h_{a_{t-1}}$  represents the node embedding corresponding to the selected operation  $a_{t-1}$  at the previous time step  $t-1$ . To handle  $h_{a_0}$ , where no previous action exists, the policy decoder uses learnable parameter, called a dummy node embedding. Since  $\text{MLP}(s_t^u) \in \mathbb{R}^{d_{\text{latent}}}$ , we have  $\mathbf{c}_t, \mathbf{k}_t^u \in \mathbb{R}^{2d_{\text{latent}}}$ .  $\mathbf{c}_t$  and  $\mathbf{k}_t^u$  are fed into a glimpse network, which employs multi-head attention to iteratively refine queries over the context (i.e., action history in our context) and state. As these inputs pass through this network, the query is generated as follows:

$$\mathbf{q}_t^l = \sum_{m=1}^{M'} \text{Attention}(\mathbf{q}_t^{l-1} W_{m,l}^Q, \mathbf{K}_t W_{m,l}^K, \mathbf{V}_t W_{m,l}^V)$$

where  $\mathbf{q}_t^0 = \mathbf{c}_t$  and  $l$  denotes the  $l$ -th glimpse layer,  $\mathbf{K}_t$  is the state embedding matrix with its  $u$ -th row being  $\mathbf{k}_t^u$ .  $W_{m,l}^Q, W_{m,l}^K \in \mathbb{R}^{2d_{\text{latent}} \times (d_{\text{latent}} + d_{\text{glimpse}})}$ ,  $W_{m,l}^V \in \mathbb{R}^{2d_{\text{latent}} \times 2d_{\text{latent}}}$  are learnable parameter matrix.  $\text{Attention}(Q, K, V)$  is as follows:

$$\text{Attention}(Q, K, V) = \text{Softmax} \left( \text{mask}_t^1 \odot \frac{QK^\top}{\sqrt{d}} \right) V$$

where  $\odot$  indicates the element-wise product and  $d$  is the  $d_{\text{latent}}/m$  and  $\text{mask}_t^1$  is a masking vector with size  $nm$ , whose  $u$ -th element indicates whether  $O_u$  is scheduled (if already selected as an action at the previous time step, a very small number, e.g.,  $-10^8$ , is used, otherwise 1). After  $L$  iterations of glimpse refinement, the logit calculator generates a logit for each operation  $O_u$  as follows:

$$\mathbf{z}_{u,t} = \text{LC}(\mathbf{q}_t^L W_{\text{LC}}^Q, \mathbf{k}_t^u W_{\text{LC}}^K)$$

where  $W_{\text{LC}}^Q, W_{\text{LC}}^K \in \mathbb{R}^{2d_{\text{latent}} \times (d_{\text{latent}} + d_{\text{logit}})}$  and logit calculating function  $\text{LC}$  with tanh clipping is defined as follows:

$$\text{LC}(q, k_u) = \begin{cases} C \cdot \tanh(\frac{q^\top k_u}{d_{\text{latent}}}) & \text{if } O_u \in \mathcal{A}(s_t) \\ -\infty & \text{otherwise} \end{cases}$$

Finally, the probability of selecting  $O_u$  in  $s_t$  is determined by the softmax function as follows:

$$p_\theta(a_t = O_u | z, s_t, a_{t-1}) = \frac{\exp^{\mathbf{z}_{u,t}}}{\sum_{u'} \exp^{\mathbf{z}_{u',t}}}$$

where  $\theta$  is the collection of parameters approximating  $\pi$ . During training, actions are sampled from this probability distribution to maintain exploration (stochastic policy), while during test, the action with the highest probability is selected deterministically (greedy policy).

### 5.3 Practical implementation

For the practical implementation of the first component of the reconstruction loss in (2),  $\mathbb{E}_{z,a \sim q}[\log p(G|z)]$ , we approximate the likelihood  $p(G|z)$  as  $p(G|\tilde{G})$ , where  $\tilde{G}$  represents the reconstructed instance generated by the decoder. This objective is then decomposed into two reconstruction losses for nodes and edges, denoted as  $\mathcal{L}_{\text{node}} + \mathcal{L}_{\text{edge}}$ . By assuming a Bernoulli distribution for the generation process, these terms are formulated as the binary cross-entropy loss:

$$\begin{aligned} \mathcal{L}_{\text{edge}} &= -\frac{1}{k^2} \sum_{e=1}^3 \sum_{i=1}^k \sum_{j=1}^k \left[ \mathbf{A}_{i,j}^{(e)} \log \mathbf{P}_{\text{edge},(e)}^{(i,j)} + (1 - \mathbf{A}_{i,j}^{(e)}) \log(1 - \mathbf{P}_{\text{edge},(e)}^{(i,j)}) \right] \\ \mathcal{L}_{\text{node}} &= -\frac{1}{k} \sum_{f=1}^6 \sum_{i=1}^k \left[ \mathbf{X}_{i,f} \log \mathbf{P}_{\text{node}}^{(i,f)} + (1 - \mathbf{X}_{i,f}) \log(1 - \mathbf{P}_{\text{node}}^{(i,f)}) \right] \end{aligned}$$

The second loss component of the reconstruction loss,  $\mathcal{L}_{\text{KL}}$ , is defined as the KL divergence between the posterior  $q_\phi(z|G)$  and the prior  $p(z)$ . To ensure computational tractability, we assume multivariate Gaussian distributions with diagonal covariance matrices, where the prior is centered at zero. Under these assumptions, the term can be computed analytically in closed form:

$$\begin{aligned} \mathcal{L}_{\text{KL}} &= D_{\text{KL}}[q_\phi(z|G) || p(z)] \\ &= \frac{1}{2} \sum_{i=1}^d \left[ \frac{\sigma_q^2}{\sigma_p^2} + \frac{\mu_{\phi_2,i}^2(h_{\text{stat}})}{\sigma_p^2} - 1 - \log \frac{\sigma_q^2}{\sigma_p^2} \right] \end{aligned}$$

The policy loss term  $\mathcal{L}_{\text{policy}}$  is derived from (4). Since the JSSP operates in a discrete action space, we can optimize the objective directly without relying on the reparameterization trick, unlike continuous control methods such as Soft Actor-Critic (SAC) or Deep Deterministic Policy Gradient (DDPG). By applying the Policy Gradient Theorem, we reformulate the objective into the following gradient form:

$$\mathcal{L}_{\text{policy}} = \mathbb{E}_{G \sim p, z, a \sim q}[\log \pi_\theta(a|z, G) A(z, a) - \alpha_{\text{entropy}} \log \pi_\theta(a|z, G)]$$

Here,  $A(z, a) = Q(z, a) - V_\gamma(z)$  denotes the advantage function.  $V_\gamma(z)$  represents the soft state value function estimating the expected return from the latent state  $z$ , while the Q-value is defined as the negative makespan,  $Q(z, a) = -C_{\text{max}}(z, a)$ . The critic loss function for policy evaluation is defined as follows:

$$\mathcal{L}_{\text{critic}} = \mathbb{E}_{G \sim p, z, a \sim q} \left[ (V_\gamma(z) - (Q(z, a) - \alpha_{\text{entropy}} \log \pi_\theta(a|z, G)))^2 \right]$$

This optimization process provides theoretical guarantees equivalent to those of Soft Policy Iteration (Details are provided in the Supplementary Material C).

The proposed method addresses the non-stationarity problem through a two-phase training approach, as outlined in **Algorithm 1**. Phase 1 trains the variational graph encoder. For each epoch, a JSSP instance is sampled (Line 3), followed by sampling of its corresponding latent variable (Line 4). The representation loss  $\mathcal{L}_{\text{repr}}$  is computed (Lines 5-7) and used to update the variational graph encoder parameters (Line 8). Upon completion of Phase 1 (representation learning), the variational graph encoder parameters are frozen (Line 11) to proceed to Phase 2. Phase 2 trains the policy decoder using mini-batch learning. A JSSP instance is randomly sampled for training (Line 15), and the latent variable for that instance is sampled accordingly (Line 16). The system then performs rollouts to construct action sequences (Lines 17-20) by interacting with the JSSP environment. Both  $\mathcal{L}_{\text{policy}}$  and  $\mathcal{L}_{\text{critic}}$  are computed and used to update the policy and critic parameters respectively.

---

**Algorithm 1** Two-Phase Training Algorithm

---

**Require:** Initial parameters  $\phi, \psi, \theta, \gamma$   
**Require:** Hyperparameters: representation epochs  $E_r$ , policy epochs  $E_p$ , learning rates  $\alpha, \beta$ , mini-batch size  $B$

- 1: **Phase 1: Variational Representation Learning**
- 2: **for**  $epoch = 1$  to  $E_r$  **do**
- 3:     Sample random JSSP instance  $G \sim p(G)$
- 4:      $z \sim q_\phi(z|G)$  {Sampling latent variable}
- 5:      $\mathbf{P}_{\text{node}}, \mathbf{P}_{\text{edge}} = g_\psi(z)$  {Reconstructing instance}
- 6:     Compute  $\mathcal{L}_{\text{KL}}$ ,  $\mathcal{L}_{\text{node}}$  and  $\mathcal{L}_{\text{edge}}$
- 7:      $\mathcal{L}_{\text{repr}} \leftarrow \mathcal{L}_{\text{KL}} + \mathcal{L}_{\text{node}} + \mathcal{L}_{\text{edge}}$
- 8:      $\phi \leftarrow \phi - \alpha \nabla_\phi \mathcal{L}_{\text{repr}}$
- 9: **end for**
- 10: **Phase 2: Policy Learning**
- 11: Fix  $\phi$  from Phase 1
- 12: **for**  $epoch = 1$  to  $E_p$  **do**
- 13:     Initialize  $\mathcal{L}_{\text{policy}} = 0$  and  $\mathcal{L}_{\text{critic}} = 0$
- 14:     **for**  $batch = 1$  to  $B$  **do**
- 15:         Sample random JSSP instance  $G \sim p(G)$
- 16:          $z \sim q_\phi(z|G)$  {Sampling latent variable}
- 17:         **for**  $t = 1$  to  $T - 1$  **do**
- 18:             **if**  $t = 1$  **then**
- 19:                  $s_1 \leftarrow g_0(G)$  {Initialize state}
- 20:             **end if**
- 21:              $a_t \sim p_\theta(a_t|z, s_t, a_{t-1})$  {Sample action}
- 22:              $s_{t+1} \leftarrow g_1(s_t, a_t, G)$  {Update state}
- 23:         **end for**
- 24:          $a = (a_1, a_2, \dots, a_{T-1})$  {Construct action sequence}
- 25:          $Q(z, a) \leftarrow -C_{\text{max}}(z, a)$  {Negative makespan}
- 26:          $V_\gamma(z) \leftarrow \text{critic network output}$
- 27:          $A(z, a) \leftarrow Q(z, a) - V_\gamma(z)$  {Advantage}
- 28:         Compute batch losses  $\mathcal{L}_{\text{policy}}, \mathcal{L}_{\text{critic}}$
- 29:          $\mathcal{L}_{\text{policy}} \leftarrow \mathcal{L}_{\text{policy}} + \frac{1}{B} \mathcal{L}_{\text{policy}}$
- 30:          $\mathcal{L}_{\text{critic}} \leftarrow \mathcal{L}_{\text{critic}} + \frac{1}{B} \mathcal{L}_{\text{critic}}$
- 31:         **end for**
- 32:          $\theta \leftarrow \theta + \beta \nabla_\theta \mathcal{L}_{\text{policy}}$  {Update policy}
- 33:          $\gamma \leftarrow \gamma - \beta \nabla_\gamma \mathcal{L}_{\text{critic}}$  {Update critic}
- 34: **end for**

---

## 6 Experiment

This section provides a multifaceted validation of the proposed VG2S framework. Our experimental evaluation is designed to assess the performance against baseline algorithms, the effectiveness of variational representation learning, the characteristics of the latent space, and the strategic behavior of the learned policy. In Section 6.1, we demonstrate the zero-shot generalization and scalability of the proposed model using various benchmark datasets. Section 6.2 presents an ablation study to analyze the impact of the VAE structure on policy optimization and training stability,

confirming its robustness across different problem scales. In Section 6.3, we utilize the UMAP algorithm to visualize the evolution of the latent space during training, illustrating how the model captures and clusters the structural features of JSSP instances. Finally, Section 6.4 provides an in-depth analysis of how the learned policy dynamically combines and utilizes the characteristics of traditional heuristics, such as SPT and MWKR, depending on the current scheduling state.

For each experiment, the proposed VG2S is trained using a dynamic data generation strategy rather than a fixed training set. Specifically, training instances are regenerated every five epochs according to the following configurations:

- **Processing time:**  $p_{ij} \sim \mathcal{DU}(1, 99)$  for each operation.
- **Number of machines:**  $m \sim \mathcal{DU}(5, 9)$ .
- **Number of jobs:**  $n \sim \mathcal{DU}(m, 9)$ .
- **Machine sequence:** A random permutation for each job, ensuring no recirculation.

where  $\mathcal{DU}(a, b)$  denotes the discrete uniform distribution between  $a$  and  $b$ . The key hyperparameters used in these experiments are optimized via grid search. Details of the hyperparameter search are provided in the Supplementary Material D.

## 6.1 Test

To evaluate the robustness of VG2S, we assess its performance across a wide range of standard JSSP benchmark instances. This involves assessing the model’s ability to maintain scheduling quality as the problem scale—number of jobs and machines—increases, as well as its zero-shot capability on diverse benchmarks. These evaluations are conducted using the model from the 6,001st policy learning epoch with hyperparameter ID 4 ( $E_r = 80,000$ ), as detailed in the Supplementary Material D. We evaluate the performance using the optimality gap metric, calculated as the percentage deviation from the best-known solution: Optimality Gap Metric:  $100\% \times \frac{C_{\max}^{\text{method}} - C_{\max}^{\text{UB}}}{C_{\max}^{\text{UB}}}$ , where  $C_{\max}^{\text{method}}$  and  $C_{\max}^{\text{UB}}$  are the makespan of the each methodology and the best-known, respectively.

### 6.1.1 Scalability test

The proposed method is evaluated on the Taillard (TA) benchmark dataset, a standard benchmark for classical JSSP. The TA01-80 instances were originally proposed in [38]. With processing time and machine sequence distributions similar to our training dataset but larger problem sizes, this dataset serves as an effective benchmark for evaluating scalability<sup>2</sup>.

For comparison, we employ priority dispatching rules (PDRs) including SPT (shortest processing time), LPT (longest processing time), SRM (shortest remaining machining time), and SRPT (shortest remaining processing time), as well as state-of-the-art DRL-GNN based algorithms from Zhang [A] [20], Park [16], Yuan [26], Liu [24], and Zhang [B] [23].

Table 1 presents the performance comparison on the TA benchmark dataset. The proposed VG2S demonstrates superior performance across the TA benchmark instances, achieving the best results in 12 out of 16 test cases (75%). Compared to priority dispatching rules (SPT, LPT, SRM, SRPT), the proposed approach consistently outperforms across all datasets. Furthermore, it surpasses state-of-the-art DRL-GNN baselines in most cases. Notably, a distinct pattern emerges when examining performance across different problem sizes. On smaller instances ( $30 \times 15$  or below), the method achieves best performance on 5 out of 8 datasets, whereas on larger instances ( $30 \times 20$  or above), it achieves best performance on 7 out of 8 datasets. This trend demonstrates that the method exhibits robust scalability, maintaining and even improving its competitive advantage as problem complexity increases.

### 6.1.2 Generalization and scalability test

To extend the evaluation scope beyond the TA dataset, which shares similar processing time and machine sequence distributions with our training data but with larger problem sizes, we additionally tested our method on widely-used benchmark datasets: DMU [39], SWV [40], LA [41], ORB [42], ABZ [19], FT [43], and YN [44]. Notably, the DMU and SWV datasets include the more challenging two-set JSSP instances. We compare our approach against recent baselines that employ reinforcement learning and GNN-based methods Chen [31], Zhang [20], Park [A] [16], Park [B]

<sup>2</sup>The dataset characteristics are as follows: the number of machines  $m$  and jobs  $n$  are drawn from  $U[15, 20]$  and  $U[15, 100]$ , respectively, while processing times are sampled from  $U[1, 99]$ . The machine operation sequences are generated through the following procedure: (1) operations are initially assigned to machines sequentially without perturbation, where the first machine processes the first operation; (2) starting from the first operation, the assigned machine is swapped with a randomly selected machine from the subsequent operations, and this procedure is repeated until the last operation.

Table 1: Performance comparison of VG2S and baseline methods on the Taillard benchmark instances

Instance	Size	SPT	LPT	SRM	SRPT	MWKR	Zhang [A] [20]	Park [16]	Yuan [26]	Liu [24]	Zhang [B] [23]	VG2S
TA01	$15 \times 15$	52.1	47.2	75.7	74.5	16.7	17.2	<b>12.8</b>	18.4	21.2	16.6	15.5
TA02	$15 \times 15$	53.8	25.6	45.8	69.9	22.9	24.1	22.1	17.3	14.5	16.2	<b>11.1</b>
TA11	$20 \times 15$	67.5	56.0	73.4	80.0	26.5	32.2	19.8	22.3	29.1	25.4	<b>14.6</b>
TA12	$20 \times 15$	84.9	61.9	79.9	58.0	25.3	32.0	22.0	20.4	23.8	27.7	<b>15.3</b>
TA21	$20 \times 20$	51.5	63.9	87.0	80.0	21.2	37.1	33.9	20.8	27.7	30.0	<b>12.6</b>
TA22	$20 \times 20$	56.9	57.2	74.8	70.4	26.3	31.4	28.1	<b>14.3</b>	20.3	23.1	15.0
TA31	$30 \times 15$	69.7	46.8	75.8	78.9	28.7	45.4	27.6	26.1	29.1	24.5	<b>21.4</b>
TA32	$30 \times 15$	71.0	47.1	77.5	83.4	25.8	33.9	33.3	23.5	<b>23.5</b>	33.5	25.8
TA41	$30 \times 20$	54.9	57.4	73.7	61.2	31.3	33.0	32.4	25.3	34.6	34.1	<b>22.9</b>
TA42	$30 \times 20$	94.7	73.3	88.0	87.1	24.0	37.5	33.1	21.9	35.4	32.8	<b>17.0</b>
TA51	$50 \times 15$	61.4	40.6	51.2	61.0	29.9	30.4	<b>13.9</b>	25.9	30.7	27.8	17.5
TA52	$50 \times 15$	51.6	41.2	66.5	58.6	25.2	21.2	14.6	23.8	27.9	25.7	<b>12.6</b>
TA61	$50 \times 20$	56.9	55.8	75.2	75.8	21.0	27.4	19.4	17.3	23.7	24.5	<b>13.0</b>
TA62	$50 \times 20$	71.9	53.9	66.1	68.0	21.6	26.1	26.4	23.7	24.0	26.5	<b>16.0</b>
TA71	$100 \times 20$	43.3	27.2	44.9	48.6	8.9	18.1	9.1	11.6	15.1	12.3	<b>7.1</b>
TA72	$100 \times 20$	46.9	28.8	46.8	47.4	8.6	9.9	6.6	10.2	15.8	9.1	<b>6.2</b>

[45], Yuan [26], Oh [32].

Table 2 presents a comprehensive performance comparison of VG2S against the baselines, covering a total of 242 benchmark datasets grouped by instance and size (Individual test results are provided in the Supplementary Material E). We evaluate the models using the optimality gap metric. The proposed VG2S achieves the best performance on 55.0% (19 out of 34) of the total benchmark dataset groups. We analyze the results from two perspectives: generalization and scalability.

First, to validate the generalization capability, we focus on the performance on the DMU and SWV datasets, which are 2-set JSSP<sup>3</sup> instances with distributions different from the training dataset. It is noteworthy that many instances in the DMU and SWV datasets remain unsolved optimally [34] and are widely recognized as particularly challenging problems [39, 40]. Despite this difficulty, the proposed method demonstrates superior performance on 90.9% (10 out of 11) of the DMU and SWV groups. These results strongly suggest that the proposed methodology exhibits excellent generalization capability, even when applied to problem distributions that differ significantly from the training data.

To assess scalability, we analyze performance based on problem size by dividing instances into two categories: those with fewer than 40 jobs and those with 40 or more jobs. For small-scale problems (fewer than 40 jobs), the baseline methods achieve the best performance in 12 out of 26 instance groups (46.2%). While the proposed method demonstrates superior performance, the margin of superiority is not substantial. In contrast, the proposed VG2S demonstrates superior performance in all 8 instance groups (100%) for large-scale problems (40 or more jobs), confirming its excellent scalability for larger problem sizes. In summary, the results show that VG2S is effective for challenging and large-scale JSSP tasks, where standard DRL models often show limited performance.

<sup>3</sup>The 2-set JSSP instances are defined by partitioning the set of machines into two distinct groups. All jobs are required to visit every machine in the first set in a random order before they can proceed to any machine in the second set. This specific routing structure has been found to be more difficult to solve than standard problems where the routings are a simple random permutation of all machines.

Table 2: Comprehensive performance evaluation of VG2S across diverse JSSP benchmarks: Generalization results on multiple instances of varying scales

Instance	Size	FIFO	MWKR	Chen [31]	Zhang [A][20]	Park [A][16]	Park [B][45]	Yuan [26]	Oh [32]	Zhang [B][23]	VG2S
TA	15 × 15	23.11	21.19	35.38	25.96	20.13	15.30	21.32	<b>14.70</b>		15.66
TA	20 × 15	30.02	22.84	32.09	30.03	24.95	19.43	22.39	16.58		<b>15.44</b>
TA	20 × 20	27.67	23.98	28.33	31.61	29.25	17.25	20.92	16.69		<b>16.30</b>
TA	30 × 15	30.22	23.96	36.43	33.00	24.70	19.09	23.28	<b>19.07</b>		19.23
TA	30 × 20	30.9	25.68	34.67	33.62	32.00	23.75	26.33	<b>19.69</b>		20.74
TA	50 × 15	20.11	17.79	31.86	20.86	15.92	13.86	16.03	13.35		<b>11.22</b>
TA	50 × 20	23.18	18.41	28.04	23.14	21.30	13.53	17.61	13.23		<b>13.22</b>
TA	100 × 20	12.75	8.81	17.98	13.52	9.24	6.66	8.91	7.17		<b>6.56</b>
DMU	20 × 15	37.18	30.49		38.95			27.74	23.14	33.52	<b>19.82</b>
DMU	20 × 20	32.43	26.35		37.74			23.56	<b>18.72</b>	28.37	19.91
DMU	30 × 15	39.29	34.79		41.86			28.70	28.04	38.24	<b>23.16</b>
DMU	30 × 20	36.57	32.18		39.48			29.21	26.55	35.64	<b>24.01</b>
DMU	40 × 15	35.08	31.16		34.50			25.32	26.83	33.79	<b>20.02</b>
DMU	40 × 20	39.72	33.24		39.00			32.47	28.28	36.45	<b>26.68</b>
DMU	50 × 15	34.74	31.04		36.20			24.96	25.75	32.67	<b>18.14</b>
DMU	50 × 20	41.38	35.34		38.40			33.42	29.89	36.85	<b>26.74</b>
SWV	20 × 10	44.4	38.71			28.42	34.39	31.42	28.28		<b>20.99</b>
SWV	20 × 15	44.93	36.71			29.39	30.51	30.89	29.94		<b>26.31</b>
SWV	50 × 10	30.04	25.61			16.80	25.33	14.10	20.68		<b>12.29</b>
LA	10 × 5	17.95	16.49			16.06	12.12	14.84	<b>9.93</b>		10.24
LA	15 × 5	9.57	5.79			1.09	2.65	7.52	<b>1.02</b>		3.32
LA	20 × 5	7.96	4.88			2.13	3.64	4.78	2.97		<b>1.80</b>
LA	10 × 10	25.32	14.82			17.06	11.95	11.65	9.99		<b>8.54</b>
LA	15 × 10	29.4	19.81			21.97	14.60	13.01	<b>11.19</b>		16.02
LA	20 × 10	24.45	20.88			27.26	15.72	17.02	<b>13.87</b>		18.70
LA	30 × 10	11.16	7.79			6.27	<b>3.10</b>	7.92	3.61		4.17
LA	15 × 15	25.29	15.83			21.40	16.07	16.22	<b>10.94</b>		14.04
ORB	10 × 10	29.73	29.93			21.83	19.98	23.08	<b>17.77</b>		18.04
ABZ	10 × 10	14.84	9.47			10.12	<b>6.15</b>	7.07	6.92		9.14
ABZ	20 × 15	31.27	21.15			29.02	20.55	22.29	19.48		<b>18.90</b>
FT	6 × 6	18.18	10.9			29.09	7.27	9.09	<b>1.82</b>		7.27
FT	10 × 10	27.31	24.94			22.80	19.46	18.49	<b>11.61</b>		13.98
FT	20 × 5	41.2	34.76			14.85	28.58	14.33	<b>8.15</b>		11.76
YN	20 × 20	25.87	20.82			24.80	18.44	20.28	17.29		<b>15.86</b>

## 6.2 Effectiveness of variational representation learning

To verify that the observed performance gains are attributable to the variational representation learning process, we perform ablation studies (Section 6.2.1) and a problem scale analysis (Section 6.2.2).

### 6.2.1 Ablation on variational representation learning

We conduct ablation experiments across four benchmark datasets: DMU76, DMU77, TA61, and TA62. We evaluated the proposed method with five different  $E_r$  values (20,000, 40,000, 60,000, 80,000, and 100,000) and compared it against a baseline model trained without the representation learning phase and reconstruction loss term. To ensure experimental robustness, we train each model configuration with six different hyperparameter combinations (The hyperparameter configuration ID 1 – 6 are provided in the Supplementary Material D). Identical hyperparameters are applied across the baseline and all  $E_r$  variants, with the only difference being the length of the representation learning process. All experiments are conducted over 20,000 policy learning epochs.

Fig. 3 illustrates these results using a moving average filter (window: 10): the solid line shows the mean performance across hyperparameter combinations at each epoch, while the shaded area denotes the interquartile range (25th to 75th percentile). Regarding learning stability, experiments across all datasets show consistent patterns: the proposed model exhibits rapid initial descent (0 - 2,000 epochs) and stable convergence, while the baseline demonstrates persistent instability with notable spikes (4,000 - 5,000). Particularly, the proposed method demonstrates relatively greater hyperparameter robustness compared to the baseline, as evidenced by the substantially narrower interquartile ranges across all datasets. In terms of final convergence values, the improvements are substantial in TA61 and DMU76, where the proposed method achieves approximately 3,200-3,300 versus baseline's 3,300-3,400 and 10,000-10,500 versus 10,500-11,000, respectively. In TA62, although the baseline shows temporary advantages at certain epochs ( $\approx 7,500$ ,  $16,000$ ,  $20,000$ ), the proposed method maintains better long-term stability and final performance. For DMU77, the baseline outperforms some  $E_r$  variants after epoch 16,000, but consistently yields higher makespan values than the best-performing configurations ( $E_r = 60,000$  and  $100,000$ ).

Overall, the experimental results validate the effectiveness of variational representation learning in enhancing the model's overall performance. This positive impact is particularly evident in three key aspects: learning stability, hyperparameter robustness, and final convergence quality.

### 6.2.2 Analysis across problem scales

To further verify the utility of variational representation learning in relation to problem scale, we conduct comprehensive testing on 463 benchmark instances spanning a wide range of problem sizes. We compared it against a baseline model trained without the representation learning phase and reconstruction loss term. For this evaluation, we selected the best-performing models based on validation performance: the baseline at the 14,401st epoch (ID 3) and the proposed VG2S at the 6,001st policy learning epoch (ID 4,  $E_r = 80,000$ ). The performance metrics are the average improvement rate with respect to problem size (red line in Fig. 4a) and the variance (blue line in Fig. 4b). The improvement rate is calculated as: Improvement Rate =  $100 \times \frac{C_{\text{baseline}}^{\text{max}} - C_{\text{proposed}}^{\text{max}}}{C_{\text{baseline}}^{\text{max}}}$ .

Fig. 4a presents the relationship between problem size (measured as  $\log(n \times m)$ ) and the improvement rate achieved by Improvement Rate. The scatter plot reveals substantial variation in performance gains across individual instances, with improvement rates ranging from approximately -10% to +12%. However, the red line representing the mean improvement rate by problem size demonstrates a clear upward trend, with a statistically significant positive correlation (Pearson  $r = 0.3243$ ,  $p < 0.001$ ). This confirms that the performance superiority of the proposed method becomes clearly evident with increasing problem scale. Notably, for smaller problems ( $\log(n \times m) < 4$ ), the mean improvement is negative or near-zero, suggesting that the baseline performs comparably or slightly better on simpler instances. However, for larger problems ( $\log(n \times m) > 5$ ), the proposed method consistently achieves positive improvements, with mean gains reaching approximately 2-3% for the largest problem sizes.

Fig. 4b provides complementary insights by examining the variance of improvement rates across problem sizes. The plot reveals a strong negative correlation (Pearson  $r = -0.7715$ ,  $p < 0.001$ ) between problem size and performance variance. For small problems ( $\log(n \times m) \approx 3.5 - 4.5$ ), the variance is exceptionally high (reaching values near 50), indicating highly inconsistent performance across different instances. In contrast, as problem size increases, the variance decreases dramatically, stabilizing below 5 for problems with  $\log(n \times m) > 6.5$ . This pattern demonstrates that for smaller instances, neither method shows consistent superiority, with highly variable performance across different problems. However, as problem scale increases, the proposed method exhibits increasingly stable and evident improvements over the baseline. Collectively, these results confirm that variational representation learning plays a critical role in performance improvement, particularly in terms of scalability as problem scale increases.

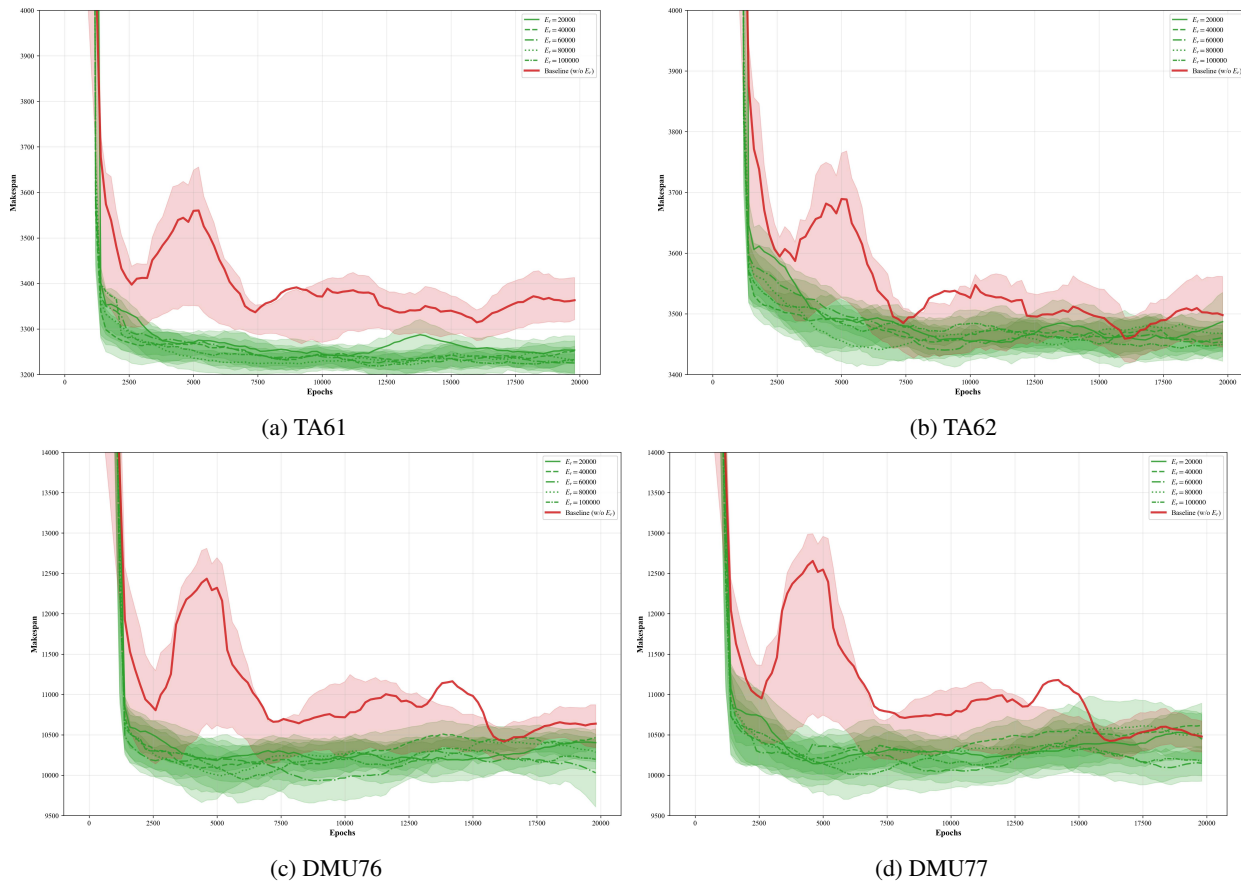


Figure 3: Learning curves showing validation performance of average makespan on benchmark datasets

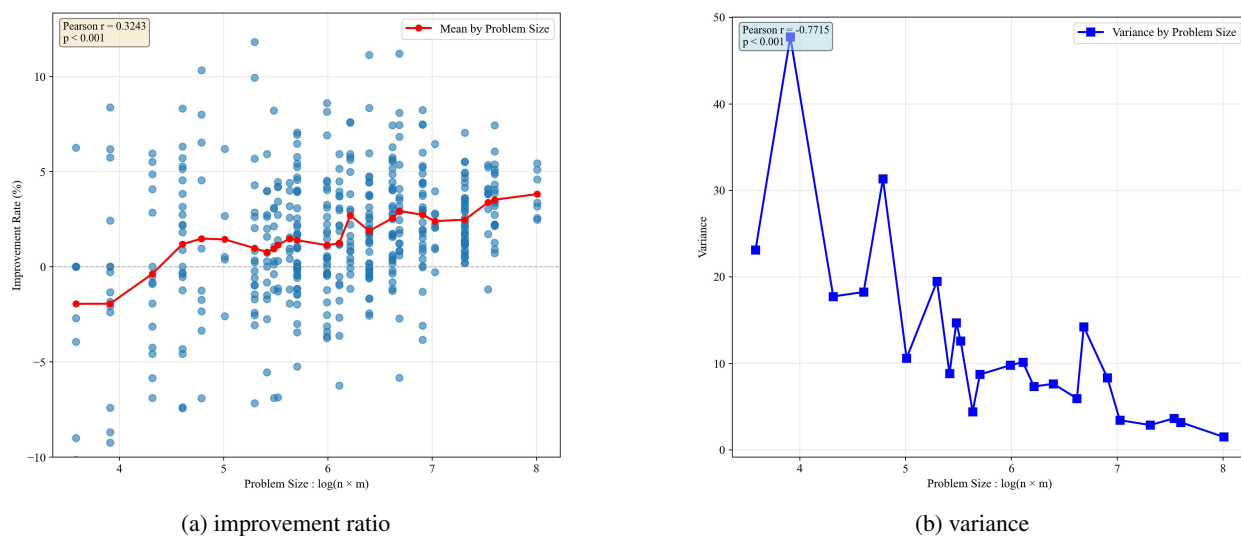


Figure 4: Trends in Improvement Rate and Performance Variance with respect to Problem Size

### 6.3 Visual analysis of latent representation via UMAP

To further investigate how the proposed framework captures the structural features of JSSP instances, we visualize the latent space using Uniform Manifold Approximation and Projection (UMAP). Fig. 5 illustrates the 2D projection of  $\mu_z$  at different training stages (Epoch 0, 6,000, and 9,000), where each point represents 20,000 JSSP instances colored by its makespan or scaled flowshop index. In this visualization, the makespan and scaled flowshop index serve as representative indicators of instance-specific characteristics. By coloring the points based on these metrics, we aim to demonstrate that the learned latent variables effectively capture and compress the essential structural features of each JSSP instance. The baseline model shares the identical architecture but is trained exclusively with the policy loss term, omitting the reconstruction loss.

**Structural awareness at initial stage (Epoch 0):** As shown in Fig. 5a and 5g, the proposed VG2S (with  $E_r = 60,000$ ) exhibits a highly organized clustering pattern even at the beginning of policy training (Epoch 0). Instances with similar makespans and scaled flowshop indices are positioned in close proximity within the latent space, forming distinct geographical clusters. In contrast, the baseline model (Fig. 5d and 5j) displays a completely stochastic distribution without any discernible pattern. This observation confirms that the variational graph encoder effectively captures the intrinsic topological properties and resource constraints of JSSP instances through representation learning, establishing a structural map prior to policy learning.

**Evolution of latent space during training (Epoch 6,000 and 9,000):** During the later stages of policy learning (Epoch 6,000 and 9,000), the proposed model maintains and further refines these structural clusters (Fig. 5b, 5c, 5h, 5i). The clear separation across different instance metrics demonstrates the representational power of the model for individual instances. In particular, from the perspective of makespan (Fig. 5b, 5c), this high expressiveness indicates that the critic can effectively guide the policy learning process by leveraging the pre-structured latent space. For the baseline model, a gradual transition in color becomes observable along UMAP Component 1 as training progresses (Fig. 5e, 5f, 5k), suggesting that the agent begins to extract some features from the reward signals. However, this pattern is significantly weaker and more fragmented compared to the proposed VG2S. Notably, as shown in Fig. 5l, the baseline fails to form a clear structural representation of the scaled flowshop index even at Epoch 9,000, suggesting that the latent space representation remains unstable even after policy learning. This suggests that the learning instability of the baseline model, as discussed in Section 6.2.1, may also stem from the instability of its latent representations. The superior clustering capability of VG2S provides a fundamental explanation for its robust zero-shot generalization. By mapping instances into a structured latent space based on their structural resemblance, the agent can immediately identify the characteristics of unseen problems. This results in more stable and efficient policy optimization compared to the baseline, which must attempt to recover structural information solely from sparse reward signals.

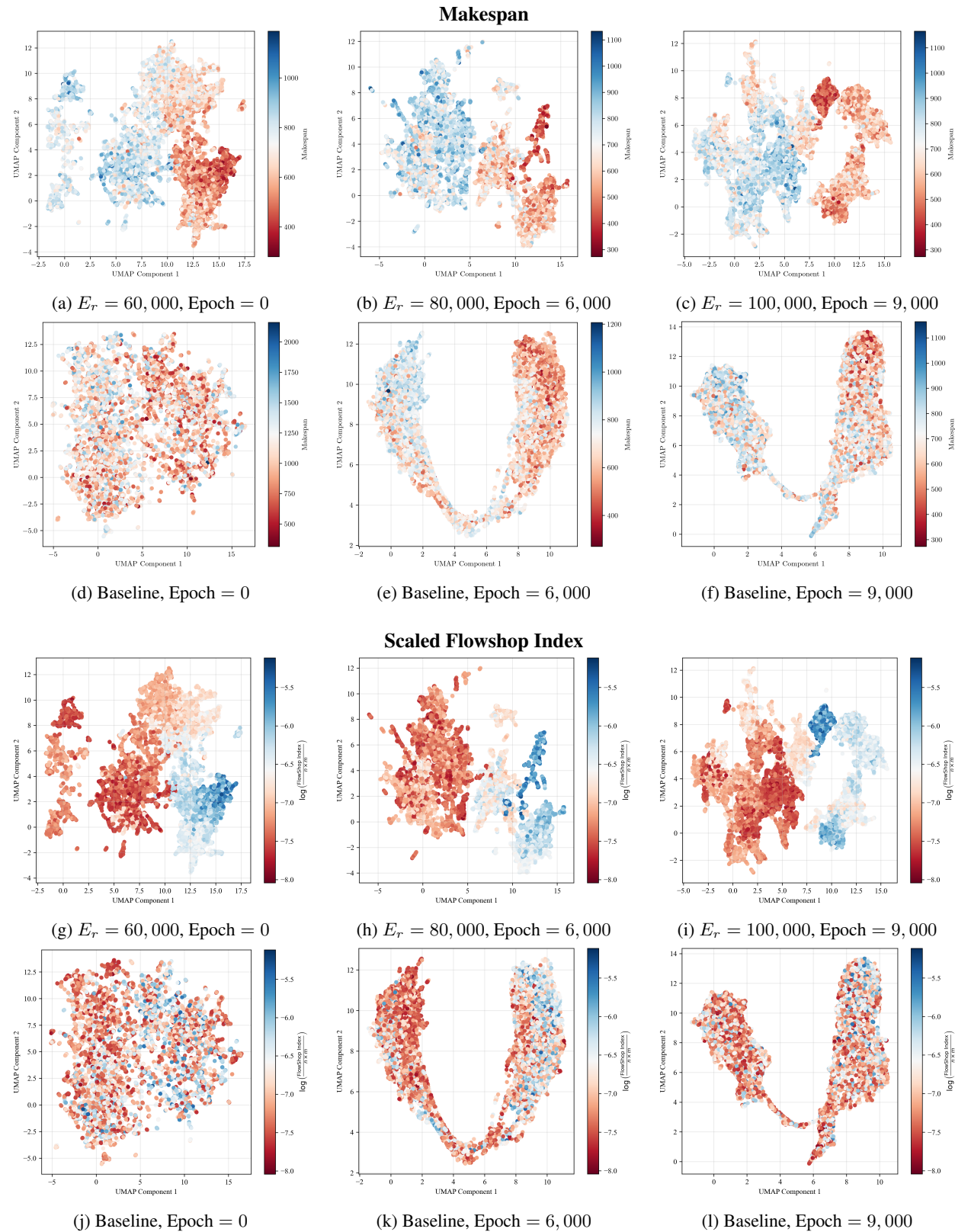


Figure 5: Latent space visualization using UMAP: Analysis of the learned manifold with points colored by makespan and scaled flowshop index

#### 6.4 Analysis of agent strategy via PDR similarity

To interpret the decision-making policy of the trained agent, we analyze its actions in terms of representative PDRs, specifically SPT and MWKR across rollouts for 100 problem instances of size  $n \times m = 200$ . In Fig. 6a, the number of completed operations denotes the number of total operations already finished for the job chosen by the policy, where a higher density of points near the origin signifies a stronger resemblance to MWKR. Similarly, in Fig. 6b, the processing time rank represents the relative rank of the processing time for the chosen operation, with clustering near the origin representing a closer alignment with SPT. As illustrated in Fig. 6, the agent does not adhere to a single rule but dynamically shifts its strategy according to the scheduling state:

**Initial phase (1–20 steps):** In the early stage, the policy exhibits high similarity to both MWKR and SPT. Since most jobs start with a large remaining workload, following the MWKR rule naturally prevents the agent from biased selection, forcing it to initiate multiple different jobs in a balanced manner. Simultaneously, the high SPT similarity indicates that the agent prioritizes operations with relatively shorter processing durations among the dispatchable set. This combined strategy allows the agent to start a wide range of job sequences early in the schedule while ensuring that machines are quickly released, maintaining the flexibility to continue this balanced distribution in subsequent steps.

**Early-mid phase (21–100 steps):** During this phase, the MWKR tendency gradually diminishes, while SPT-like behavior remains dominant. After establishing the initial skeleton of the schedule, the agent shifts its focus from total job workload to individual operation efficiency. By prioritizing shorter processing durations, the agent maximizes machine turnover—ensuring that machines become ready for the next assignment as soon as possible. This logic allows the agent to densely fill the available slots in the Gantt chart within a limited number of decision steps, effectively increasing the assignment density.

**Mid-late phase (101–180 steps):** As the assignment sequence progresses, the similarity to MWKR begins to rise again while the SPT tendency declines. As the number of available assignment steps decreases, the agent identifies jobs with many remaining operations that, if left until late in the sequence, might significantly increase the makespan. To prevent this, the policy re-prioritizes these jobs, ensuring a balanced distribution of the remaining tasks across the final stages of the schedule construction.

**Final phase (181–200 steps):** Notably, the final stage is characterized by a simultaneous peak in both MWKR and SPT similarities. This phenomenon is primarily driven by a shrinking action space. As the vast majority of operations have already been assigned, the number of candidates in the decision pool becomes extremely limited. Consequently, the few remaining operations—typically the final segments of the most work-heavy jobs—naturally align with the criteria of both MWKR and SPT, leading to a strategic convergence as the agent finalizes the schedule closure.

These results demonstrate that VG2S learns a sophisticated, time-varying policy that outperforms static heuristics by adaptively balancing workload distribution and flow efficiency. While this analysis provides qualitative insights into the agent's decision-making logic, it should be noted that the observed alignment with PDRs does not imply that a manually crafted heuristic following these phases would achieve equivalent performance. The superiority of VG2S stems from its ability to capture latent critical information that extend beyond the simplistic criteria of standard PDRs.

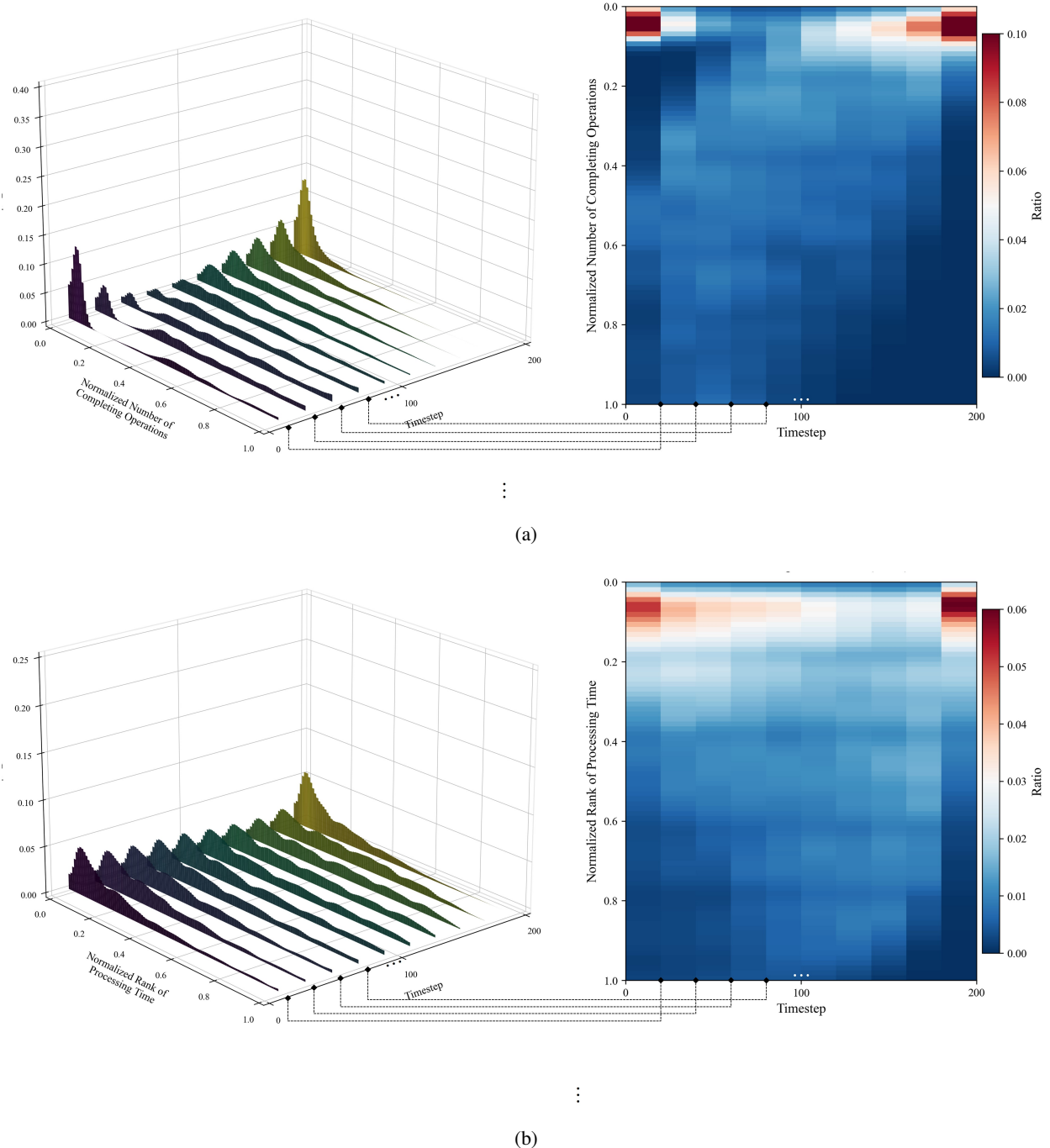


Figure 6: Visualization of policy behavior patterns

## 7 Discussion

The proposed VG2S framework demonstrates that the chronic issues of DRL in solving JSSP—specifically learning non-stationarity and limited generalization—can be effectively addressed through a probabilistic and architectural approach. We attribute these improvements to the following key factors:

1. **Decoupling representation learning from policy optimization:** While representation learning in traditional end-to-end DRL often shifts alongside policy evolution—leading to instability and non-stationarity—VG2S stabilizes the learning process by decoupling instance representation from the scheduling policy via an ELBO-based objective. Specifically, VG2S adopts a two-phase training strategy to operationalize this decoupling. The effectiveness of this combination is substantiated in Section 6.2.1, which confirms that this mathematical and temporal decoupling ensures faster convergence and robust learning stability by providing a consistent input signal to the agent.
2. **Structural manifold mapping:** VG2S maps the complex constraints of JSSP onto a structured latent manifold. As evidenced in Section 6.3, the model autonomously clusters instances based on their topological similarities. This structural awareness allows the framework to maintain high performance even as problem complexity or scale increase, a capability further validated by the results in Section 6.2.2.
3. **Probabilistic robustness against distributional shifts:** The variational approach treats the instance space as a probability distribution rather than a deterministic point. This inherent stochasticity enables the model to handle Out-of-Distribution (OOD) data more effectively. The superior zero-shot performance observed in Section 6.1.2—particularly on unseen benchmarks such as DMU and SWV—proves that VG2S captures the universal underlying logic of JSSP rather than over-fitting to specific training distributions.
4. **Context-aware strategic flexibility:** VG2S does not rely on a single fixed heuristic; instead, it dynamically composes strategies based on the current state of the manufacturing environment. Section 6.4 reveals that the agent learns to adaptively combine or outperform traditional priority rules. This strategic flexibility is crucial for real-world manufacturing scenarios where constraints and priorities shift in real-time.

## 8 Conclusion

In this study, we proposed the VG2S framework, which introduces variational inference to the JSSP domain for the first time to effectively handle problem-level uncertainty. VG2S utilizes the ELBO to mathematically decouple representation learning from policy optimization, fundamentally addressing the non-stationarity issue often encountered in DRL approaches. Experimental results demonstrated that the proposed VG2S achieves superior zero-shot generalization performance and robustness on large-scale and highly difficult benchmark datasets, such as DMU and SWV, compared to existing methods.

While this study focused on addressing uncertainty in static JSSP environments, real-world manufacturing sites frequently experience real-time dynamic events such as machine breakdowns or rush orders. Therefore, future research needs to extend VG2S to Dynamic JSSP environments to reflect these unexpected situations and adjust schedules in real-time. Furthermore, this study concentrated on single-objective optimization, specifically minimizing the Makespan. For practical application in production processes, development towards a Multi-objective Reinforcement Learning framework is required to simultaneously consider conflicting objectives such as tardiness compliance, energy efficiency, and machine utilization rates. Finally, expanding the scope of the VG2S framework to problems with more complex constraints, such as the Flexible JSSP, and verifying its versatility across various manufacturing scenarios remains an important task for future research.

## Acknowledgement

This work was supported in part by the National Research Foundation of Korea (NRF) Grant funded by the Korean Government (MSIT) under Grant RS-2025-00555741; in part by the Technology Innovation Program funded by the Ministry of Trade, Industry and Energy (MOTIE) under Grant RS-2025-02372996; and in part by the International Cooperative R&D Program funded by MOTIE and the Korea Institute for Advancement of Technology (KIAT) under Project 0022929.

## References

- [1] B. Waschneck, A. Reichstaller, L. Belzner, T. Altenmüller, T. Bauernhansl, A. Knapp, A. Kyek, Deep reinforcement learning for semiconductor production scheduling, in: 2018 29th annual SEMI advanced semiconductor manufacturing conference (ASMC), IEEE, 2018, pp. 301–306.
- [2] I.-B. Park, J. Huh, J. Kim, J. Park, A reinforcement learning approach to robust scheduling of semiconductor manufacturing facilities, *IEEE Transactions on Automation Science and Engineering* 17 (3) (2019) 1420–1431.
- [3] Y. I. Cho, S. H. Nam, K. Y. Cho, H. C. Yoon, J. H. Woo, Minimize makespan of permutation flowshop using pointer network, *Journal of Computational Design and Engineering* 9 (1) (2022) 51–67.
- [4] Z. Zong, H. Wang, J. Wang, M. Zheng, Y. Li, Rbg: Hierarchically solving large-scale routing problems in logistic systems via reinforcement learning, in: Proceedings of the 28th ACM SIGKDD Conference on Knowledge Discovery and Data Mining, 2022, pp. 4648–4658.
- [5] T. Phiboonbanakit, T. Horanont, V.-N. Huynh, T. Supnithi, A hybrid reinforcement learning-based model for the vehicle routing problem in transportation logistics, *Ieee Access* 9 (2021) 163325–163347.
- [6] H. Huang, Z. Hu, Z. Lu, X. Wen, Network-scale traffic signal control via multiagent reinforcement learning with deep spatiotemporal attentive network, *IEEE Transactions on Cybernetics* 53 (1) (2023) 262–274. doi:10.1109/TCYB.2021.3087228.
- [7] T. Tan, F. Bao, Y. Deng, A. Jin, Q. Dai, J. Wang, Cooperative deep reinforcement learning for large-scale traffic grid signal control, *IEEE Transactions on Cybernetics* 50 (6) (2020) 2687–2700. doi:10.1109/TCYB.2019.2904742.
- [8] S. H. Oh, G. W. Byeon, Y.-I. Cho, S. Kwon, J. H. Woo, Artificial intelligence in combat decision-making: weapon target assignment via reinforcement learning and graph neural networks, *IEEE Transactions on Cybernetics* (2025).
- [9] S. Li, X. He, X. Xu, T. Zhao, C. Song, J. Li, Weapon-target assignment strategy in joint combat decision-making based on multi-head deep reinforcement learning, *IEEE Access* 11 (2023) 113740–113751.
- [10] X. Wu, X. Yan, D. Guan, M. Wei, A deep reinforcement learning model for dynamic job-shop scheduling problem with uncertain processing time, *Engineering Applications of Artificial Intelligence* 131 (2024) 107790. doi:<https://doi.org/10.1016/j.engappai.2023.107790>.  
URL <https://www.sciencedirect.com/science/article/pii/S0952197623019747>
- [11] T. Gabel, M. Riedmiller, Distributed policy search reinforcement learning for job-shop scheduling tasks, *International Journal of production research* 50 (1) (2012) 41–61.
- [12] S. H. Oh, Y. I. Cho, J. H. Woo, Distributional reinforcement learning with the independent learners for flexible job shop scheduling problem with high variability, *Journal of Computational Design and Engineering* 9 (4) (2022) 1157–1174.
- [13] J. C. Serrano-Ruiz, J. Mula, R. Poler, Job shop smart manufacturing scheduling by deep reinforcement learning, *Journal of Industrial Information Integration* 38 (2024) 100582. doi:<https://doi.org/10.1016/j.jii.2024.100582>.  
URL <https://www.sciencedirect.com/science/article/pii/S2452414X24000268>
- [14] L. Wang, X. Hu, Y. Wang, S. Xu, S. Ma, K. Yang, Z. Liu, W. Wang, Dynamic job-shop scheduling in smart manufacturing using deep reinforcement learning, *Computer Networks* 190 (2021) 107969.
- [15] X. Wu, X. Yan, A spatial pyramid pooling-based deep reinforcement learning model for dynamic job-shop scheduling problem, *Computers & Operations Research* 160 (2023) 106401. doi:<https://doi.org/10.1016/j.cor.2023.106401>.  
URL <https://www.sciencedirect.com/science/article/pii/S0305054823002654>
- [16] J. Park, J. Chun, S. H. Kim, Y. Kim, J. Park, Learning to schedule job-shop problems: representation and policy learning using graph neural network and reinforcement learning, *International journal of production research* 59 (11) (2021) 3360–3377.
- [17] M. Gori, G. Monfardini, F. Scarselli, A new model for learning in graph domains, in: *Proceedings. 2005 IEEE International Joint Conference on Neural Networks, 2005.*, Vol. 2, 2005, pp. 729–734 vol. 2, doi: 10.1109/IJCNN.2005.1555942. doi:10.1109/IJCNN.2005.1555942.
- [18] P. Brucker, B. Jurisch, B. Sievers, A branch and bound algorithm for the job-shop scheduling problem, *Discrete applied mathematics* 49 (1-3) (1994) 107–127.
- [19] J. Adams, E. Balas, D. Zawack, The shifting bottleneck procedure for job shop scheduling, *Management science* 34 (3) (1988) 391–401.

[20] C. Zhang, W. Song, Z. Cao, J. Zhang, P. S. Tan, X. Chi, Learning to dispatch for job shop scheduling via deep reinforcement learning, *Advances in neural information processing systems* 33 (2020) 1621–1632.

[21] J.-P. Huang, L. Gao, X.-Y. Li, An end-to-end deep reinforcement learning method based on graph neural network for distributed job-shop scheduling problem, *Expert Systems with Applications* 238 (2024) 121756. doi:<https://doi.org/10.1016/j.eswa.2023.121756>.  
URL <https://www.sciencedirect.com/science/article/pii/S0957417423022583>

[22] J.-P. Huang, L. Gao, X.-Y. Li, A hierarchical multi-action deep reinforcement learning method for dynamic distributed job-shop scheduling problem with job arrivals, *IEEE Transactions on Automation Science and Engineering* 22 (2025) 2501–2513. doi:[10.1109/TASE.2024.3380644](https://doi.org/10.1109/TASE.2024.3380644).

[23] W. Zhang, F. Zhao, C. Yang, C. Du, X. Feng, Y. Zhang, Z. Peng, X. Mei, A novel soft actor–critic framework with disjunctive graph embedding and autoencoder mechanism for job shop scheduling problems, *Journal of Manufacturing Systems* 76 (2024) 614–626. doi:<https://doi.org/10.1016/j.jmsy.2024.08.015>.  
URL <https://www.sciencedirect.com/science/article/pii/S027861252400178X>

[24] C.-L. Liu, C.-J. Tseng, P.-H. Weng, Dynamic job-shop scheduling via graph attention networks and deep reinforcement learning, *IEEE Transactions on Industrial Informatics* 20 (6) (2024) 8662–8672. doi:[10.1109/TII.2024.3371489](https://doi.org/10.1109/TII.2024.3371489).

[25] Z. Liu, H. Mao, G. Sa, H. Liu, J. Tan, Dynamic job-shop scheduling using graph reinforcement learning with auxiliary strategy, *Journal of Manufacturing Systems* 73 (2024) 1–18. doi:<https://doi.org/10.1016/j.jmsy.2024.01.002>.  
URL <https://www.sciencedirect.com/science/article/pii/S0278612524000025>

[26] E. Yuan, S. Cheng, L. Wang, S. Song, F. Wu, Solving job shop scheduling problems via deep reinforcement learning, *Applied Soft Computing* 143 (2023) 110436.

[27] J.-P. Huang, L. Gao, X.-Y. Li, C.-J. Zhang, A novel priority dispatch rule generation method based on graph neural network and reinforcement learning for distributed job-shop scheduling, *Journal of Manufacturing Systems* 69 (2023) 119–134.

[28] S. Moon, S. Lee, K.-J. Park, Learning-enabled flexible job-shop scheduling for scalable smart manufacturing, *Journal of Manufacturing Systems* 77 (2024) 356–367.

[29] W. Zhang, F. Zhao, Y. Li, C. Du, X. Feng, X. Mei, A novel collaborative agent reinforcement learning framework based on an attention mechanism and disjunctive graph embedding for flexible job shop scheduling problem, *Journal of Manufacturing Systems* 74 (2024) 329–345.

[30] Y.-i. Cho, S.-h. Oh, J.-h. Choi, J. H. Woo, Solving quay wall allocation problems based on deep reinforcement learning, *Engineering Applications of Artificial Intelligence* 150 (2025) 110598.

[31] R. Chen, W. Li, H. Yang, A deep reinforcement learning framework based on an attention mechanism and disjunctive graph embedding for the job-shop scheduling problem, *IEEE Transactions on Industrial Informatics* 19 (2) (2022) 1322–1331.

[32] S. H. Oh, Y.-i. Cho, H. Oh, J. Baek, S. W. Han, J. H. Woo, Framework for state features design in job shop scheduling with deep reinforcement learning: Beyond empirical approaches, *Journal of Computational Design and Engineering* 13 (1) (2025) 24–44. arXiv:<https://academic.oup.com/jcde/article-pdf/13/1/24/65042073/qwaf118.pdf>, doi:[10.1093/jcde/qwaf118](https://doi.org/10.1093/jcde/qwaf118).  
URL <https://doi.org/10.1093/jcde/qwaf118>

[33] W. Zhang, F. Zhao, C. Yang, C. Du, X. Feng, Y. Zhang, Z. Peng, X. Mei, A novel soft actor–critic framework with disjunctive graph embedding and autoencoder mechanism for job shop scheduling problems, *Journal of Manufacturing Systems* 76 (2024) 614–626.

[34] J. Xie, X. Li, L. Gao, L. Gui, A hybrid algorithm with a new neighborhood structure for job shop scheduling problems, *Computers & Industrial Engineering* 169 (2022) 108205.

[35] A. X. Lee, A. Nagabandi, P. Abbeel, S. Levine, Stochastic latent actor-critic: Deep reinforcement learning with a latent variable model, *Advances in Neural Information Processing Systems* 33 (2020) 741–752.

[36] D. P. Kingma, M. Welling, Auto-encoding variational bayes, arXiv preprint arXiv:1312.6114 (2013).

[37] X. Wang, H. Ji, C. Shi, B. Wang, Y. Ye, P. Cui, P. S. Yu, Heterogeneous graph attention network, in: The world wide web conference, pp. 2022–2032.

[38] E. Taillard, Benchmarks for basic scheduling problems, *European journal of operational research* 64 (2) (1993) 278–285.

- [39] E. Demirkol, S. Mehta, R. Uzsoy, Benchmarks for shop scheduling problems, *European Journal of Operational Research* 109 (1) (1998) 137–141.
- [40] R. H. Storer, S. D. Wu, R. Vaccari, New search spaces for sequencing problems with application to job shop scheduling, *Management science* 38 (10) (1992) 1495–1509.
- [41] S. Lawrence, Resource constrained project scheduling: an experimental investigation of heuristic scheduling techniques, GSIA, Carnegie Mellon University (1984).
- [42] D. Applegate, W. Cook, A computational study of the job-shop scheduling problem, *ORSA Journal on computing* 3 (2) (1991) 149–156.
- [43] H. Fisher, G. L. Thompson, Probabilistic learning combinations of local job-shop scheduling rules, *Industrial scheduling* (1963).
- [44] T. Yamada, R. Nakano, A genetic algorithm applicable to large-scale job-shop problems, in: *Parallel Problem Solving from Nature*, 1992.  
URL <https://api.semanticscholar.org/CorpusID:37171770>
- [45] J. Park, S. Bakhtiyar, J. Park, Schedulenet: Learn to solve multi-agent scheduling problems with reinforcement learning, *arXiv preprint arXiv:2106.03051* (2021).